Journal Pre-proof

Gain-of-function CFTR restores essential epithelial function with greater efficacy than wildtype or codon optimized CFTR when expressed in cystic fibrosis airway cells.

Maximillian Woodall, Robert Tarran, Rhianna Lee, Hafssa Anfishi, Stella Prins, John Counsell, Paola Vergani, Stephen Hart, Deborah Baines

PII: S2329-0501(23)00120-1

DOI: https://doi.org/10.1016/j.omtm.2023.08.006

Reference: OMTM 1087

To appear in: *Molecular Therapy: Methods & Clinical Development*

Received Date: 21 February 2023

Accepted Date: 10 August 2023

Please cite this article as: Woodall M, Tarran R, Lee R, Anfishi H, Prins S, Counsell J, Vergani P, Hart S, Baines D, Gain-of-function CFTR restores essential epithelial function with greater efficacy than wildtype or codon optimized CFTR when expressed in cystic fibrosis airway cells., *Molecular Therapy: Methods & Clinical Development* (2023), doi: https://doi.org/10.1016/j.omtm.2023.08.006.

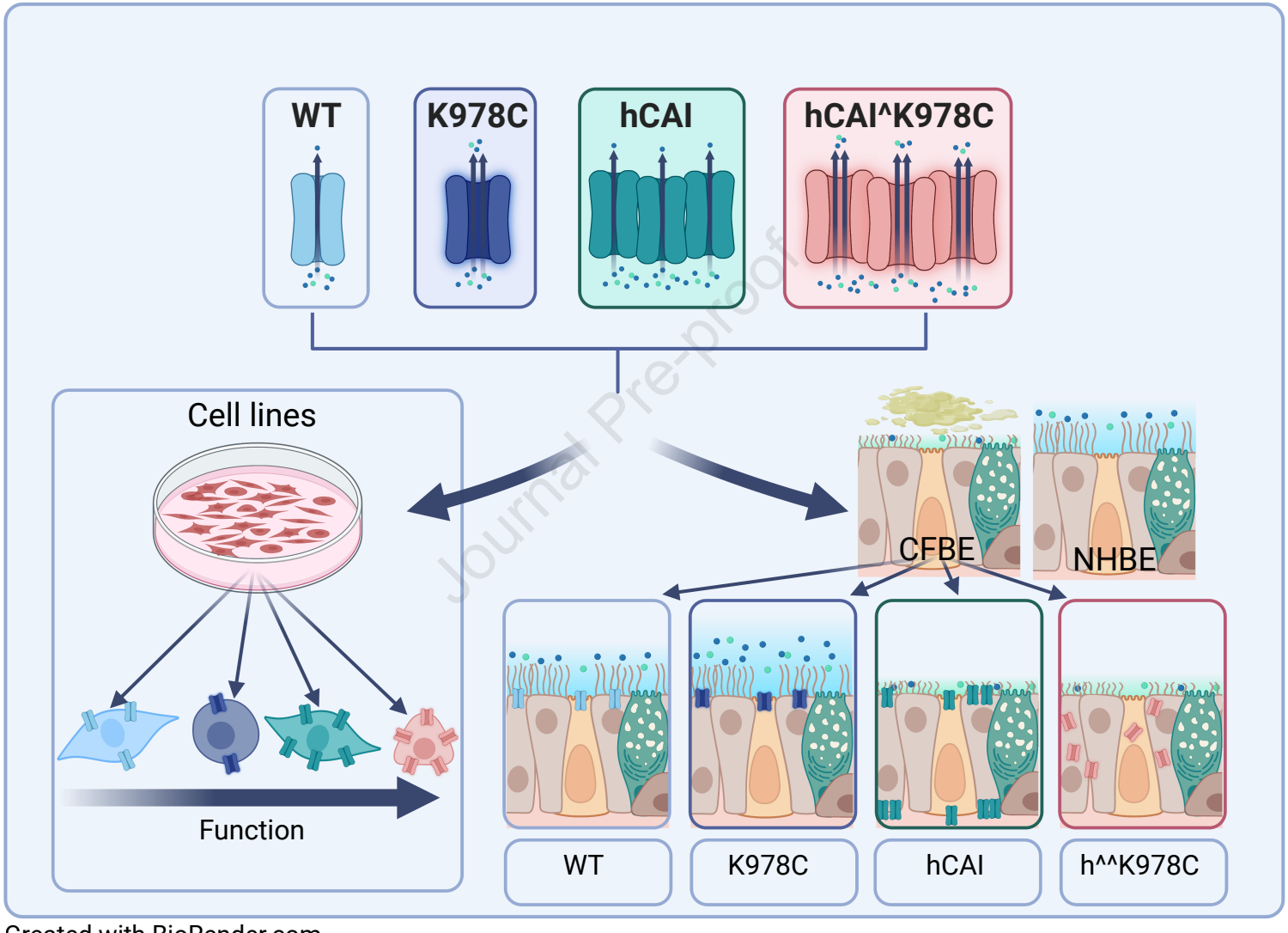

Created with BioRender.com

Gain-of-function CFTR restores essential epithelial function with greater efficacy than wildtype or codon optimized CFTR when expressed in cystic fibrosis airway cells.

Maximillian Woodall[1], Robert Tarran[2], Rhianna Lee[2], Hafssa Anfishi[1], Stella Prins[3], John Counsell[4], Paola Vergani[3], Stephen Hart[4], Deborah Baines[1]

[1]Institute for Infection and Immunity, St George's, University of London, Cranmer Terrace, Tooting, London SW17 0RE, UK . [2]Department of Cell Biology & Physiology, University of North Carolina at Chapel Hill, NC 27599-7248, USA. [3]Neuroscience, Physiology & Pharmacology, Division of Biosciences, University College London, London WC1E 6BT, UK.[4] Genetics & Genomic Medicine Dept, Great Ormond Street Institute of Child Health, London WC1N 1EH, UK.

* Deborah Baines; Institute for Infection and Immunity, St George's, University of London, Cranmer Terrace, Tooting, London SW17 0RE.

Email: dbaines@sgul.ac.uk

Abstract

Class Ia/b cystic fibrosis transmembrane regulator (CFTR) variants cause severe lung disease in 10% of cystic fibrosis (CF) patients and are untreatable with small molecule pharmaceuticals. Genetic replacement of CFTR offers a cure, but its effectiveness is limited *in vivo*. We hypothesized that enhancing protein levels (using codon optimisation) and/or activity (using gain-of-function variants) of CFTR would more effectively restore function to CF bronchial epithelial cells. Three different variants of the CFTR protein were tested: codon optimized (hCAI), a gain-of-function (GOF) variant (K978C), and a combination of both (h^K978C). In human embryonic kidney cells (HEK293T), initial results showed that hCAI and h^K978C produced >10-fold more CFTR protein and displayed ~4-fold greater activity than WT-CFTR. However, functionality was profoundly different in CF bronchial epithelial cells. Here, K978C-CFTR more potently restored essential epithelial functions (anion transport, airway surface liquid height and pH) than WT CFTR. hCAI and h^K978C-CFTRs had limited impact due to mis-localization in the cell. These data provide proof of principle that GOF variants may be more effective than codon optimised forms of CFTR for CF gene therapy.

Introduction

Precision medicine, through pharmacotherapy, has revolutionized the treatment of cystic fibrosis transmembrane regulator (CFTR) variants that exhibit recoverable CFTR protein. Nevertheless, class Ia (no mRNA) and class Ib (no protein) mutations, which are responsible for about 10% of all CF-causing CFTR variants, remain untreatable[1]. Gene therapy and gene editing techniques, whilst still in their infancy, hold immense promise as a potential cure for all forms of CF, including class-I mutations. Proof-of-concept studies have established feasibility of genetic therapies, but the limited success of CF gene therapy clinical trials highlights the need for further development and understanding of these techniques.

The estimated level of functional endogenous CFTR required to ameliorate severe pulmonary disease *in vivo*, range from 5% and 16% [2–6] , a level yet to be achieved in clinical trials. *In vivo* delivery of airway-targeted genetic therapies faces significant challenges due to natural airway barriers, which hinder the delivery and overall potency of genetic therapy formulations[5,7,8]. *In vitro*, where it is easier to manipulate target cells, the presence of 10-60% endogenous expression of CFTR was required to recapitulate normal anion transport function[9–11] whereas transduction of only 6-25% CF cells with exogenous wild type (WT) CFTR cDNA, generated Cl^- transport properties similar to non-CF cultures[12,13]. However, none of the above studies considered the

impact of the CF luminal environment on CFTR and epithelial function, therefore these estimates may not translate *in vivo*.

Several innovative strategies are being developed to enhance the potency of gene therapy for CF. For instance, codon optimization of CFTR has been employed to reduce the immunogenicity of the DNA used in gene therapy by depleting cytosine-phosphorothioate-guanine (CpG) motifs, which stimulate the toll-like receptor 9 (TLR9) inflammatory pathway[14–16]. Codon optimization also enhances the translation of mRNA into protein by substituting rare codons (triplets of DNA bases that code for amino acids less frequently within a specific organism) which can decelerate or even halt the translation process [17,18]. The replacement of the rare codons in WT-CFTR increased protein production and function dramatically (>10 fold) when expressed in Fisher Rat Thyroid cells[18]. However, research into codon-optimized CFTR function in human airway cells is relatively nascent, with current findings mostly reporting mild changes in CFTR-mediated anion transport and no data on airway surface liquid (ASL) rehydration is yet available[19]. The potential of using gain-of-function (GOF) CFTR mutants as a strategy for improving CF gene therapy remains largely unexplored. Study of CFTR structure and function relationships identified several such mutations[20,21]. One mutation, K978C-CFTR, demonstrated >2-fold higher open probability (P_o) in excised patch-clamp studies than WT-CFTR[21–23]. Studies of GOF CFTRs have so far been limited to functional testing in cell lines. However, CF bronchial epithelial cells (CFBE) grown at

the air-liquid-interface are considered the gold standard for preclinical airway model systems [24,25]. In these cells, the function and effectiveness of GOF CFTRs such as K978C-CFTR for genetic therapy practices is uncharted. K978C was selected over other GOF variants for the unique characteristics of an increased Po while retaining regulation by cAMP/PKA[21].

We hypothesised that the use of a codon-optimized form of CFTR, K978C-CFTR, or codon-optimized K978C-CFTR could improve the performance of CF gene therapy in a physiologically relevant model. We first investigated protein production and function of our CFTR constructs in HEK293T cells. This provided us with a basic understanding of construct behavior in a reproducible cell line environment. Next, we transitioned our research to primary airway epithelial cells, using non-CF (NHBE) and CF Class 1 (W1282X/R1162X) and F508del genotypes (CFBE). We introduced and examined the protein production and localisation of the exogenously expressed, CFTR constructs each controlled by a high-activity promoter. In the final stage, we analyzed the function of CFTR constructs in differentiated CFBE cells and compared them to the function of endogenous CFTR from mixed cultures of NHBE and CFBE. Importantly, the functional tests were performed in the presence of CF sputum as our previous research indicated that CF sputum inhibits CFTR function and disrupted normal ASL hydration compared to normal lung sputum[26]. Our objective was to identify the transduction efficiency required to restore CFTR-dependent

anion transport and ASL hydration to that of NHBE in the presence of normal lung sputum as a criteria for therapeutic success[26].

Results

Expression and function of CFTR cDNAs in HEK293T cells

All CFTR constructs (Fig. 1Ai), were transfected into human embryonic kidney HEK293T cells to investigate expression and function (Fig. 2Aii). All CFTR variants produced protein, visible as the mature, complex glycosylated ~170kDa protein (band C), and immature core glycosylated ~140 kDa protein (band B) by western blot (Fig. 1B). The halide-sensitive YFP (HS-YFP) protein in co-transfected HEK293T cells was observed at ~22 kDa. Transfection of HEK293T with codon optimised hCAI- and h^K978C-CFTR resulted in >10-fold more CFTR protein than WT-CFTR (14.37±2.2 and 11.21±1.50 fold respectively $p<0.05$; n=3) (Fig. 1C). There was no significant difference in abundance of K978C- compared to WT-CFTR protein. A HS-YFP fluorescence quenching assay was employed to determine the anion transport function of CFTRs with increased abundance (Fig. 1D-F). There was little decrease of HS-YFP fluorescence in the presence of DMSO (vehicle), providing evidence that the K978C GOF mutation did not result in constitutive activity (Fig. 1D). Addition of CFTR activator forskolin to WT-, hCAI-CFTR and h^K978C-CFTRs transfected HEK293T cells produced a decrease in HS-YFP fluorescence (Fig. 1E). h^K978C-CFTR displayed significantly greater maximal rate of I^- entry compared to hCAI-CFTR

(0.3 mM/s and 0.23 mM/s, respectively; $p<0.05$; n=3), and WT-CFTR (0.06 mM/s, $p<0.001$, n=3) (Fig. 1G, Fig. S1). Prior exposure of hCAI-CFTR to potentiator VX770 increased quenching of HS-YFP fluorescence (n=3, $p<0.01$) producing a similar maximal rate of I^- entry to h^K978C-CFTR (Fig. 1F and G). WT maximal rate of iodide entry was also increased >2-fold (0.057±0.011 mM/s to 0.15±0.012 mM/s, $p<0.01$; n=3) (S1) though this remained lower than hCAI-CFTR or h^K978C-CFTR (0.15 mM/s, 0.30 mM/s and 0.32 mM/s respectively, $p<0.05$; n=3) (Fig. 2G) (Fig. S1).

Protein expression and localisation of CFTR cDNAs in CFBE.

Transduction of CFBE with all CFTR cDNAs produced distinct CFTR proteins, mature (band C ~170kDa), immature (band B ~140kDa) (Fig. 2A). As expected, hCAI-CFTR produced the most CFTR protein per transduced cell ($p<0.001$, n=5-7 from 3 donors). However, h^K978C-CFTR produced less CFTR protein than WT ($p<0.05$, n=4-7 from 3 donors). The abundance of band C was more than 5-fold higher than that of band B, (ratio: 5.1-5.2) across all forms of CFTR ($p<0.05$, n=4-7 from 3 donors) except for h^K978C-CFTR (Fig. 2B). To address potential protein aggregation often associated with high protein yields, we employed two strategies on the h^K978C transduced cells: we raised the denaturation temperature of the protein lysate to 80°C from 37°C (Fig. S2B) and tested the Triton-X100 insoluble fraction with a stronger detergent, SDS, to detect any trapped protein (Fig. S2). These modifications resulted in further reduction in CFTR band

intensity, suggesting that the protein was not sequestered in aggregates but indeed expressed at a lower level. The amount of GFP in the cell broadly followed the same pattern except that GFP for codon optimized h^K978C-CFTR was higher than for K978C-CFTR ($p<0.05$, n=4-7 from 3 donors) (Fig. S2D).

We then employed CFTR constructs with GFP fused to the CFTR N-terminus to further investigate protein localisation in F508del/F508del CFBE transduced with BMI-1 (CFBE BMI-1). CFBE BMI-1 are functionally similar to primary CFBE but have extended proliferative capacity[27]. This enabled reproducible acquisition of fluorescent images and fluorescence recovery after photobleaching (FRAP) data across cell passages. WT and K978C-CFTR GFP fluorescence were clearly localised to the periphery of the cell, consistent with membrane localisation (Fig. S2E) hCAI-CFTR exhibited increased membrane and intracellular fluorescence (Fig 2C, Fig. S2E). h^K978C-CFTR was identified throughout the cell and blebbing, a characteristic marker of cell apoptosis was also observed (white arrows: Fig. 2C)[28]. FRAP was used to determine if the GFP-linked proteins displayed increased free, rapid diffusion characteristic of a non-membrane bound protein (Fig. 2D, Fig. S2F). h^K978C-CFTR displayed the characteristics of a non-membrane bound protein unlike WT-, K978C- and hCAI-CFTRs ($p<0.001$, n=8-10), (Fig. 2E and F, Fig. S2F).

Definition of models used to investigate CFTR function in primary CF bronchial epithelial cells.

Male (XY) or female (XX) donor CFBE or NHBE were isolated from bronchial regions of CF and non-CF lungs, counted and mixed at 10%, 20%, 50% and 75% (NHBE:CFBE) as represented (Fig. 3A). Markers of epithelial differentiation including cilia (a-tubulin) and F-actin structure associated with tight junctions, visualized by phalloidin, were present in all mixed-cultures (only data from 50:50 mix is shown in Fig. 3B). The final percentage of NHBE:CFBE in the co-cultures, as analyzed by droplet digital PCR for AMEL-X or AMEL-Y, was different to the original seeding percentage. This appeared to be donor-specific and independent of the CF mutation or whether the donor was male or female (Fig. 3C).

The CFTR variants were introduced into CF cells, specifically W1282X/R1162X or F508del, using a lentiviral vector. These CFTR variants were positioned upstream of a Green Fluorescent Protein (GFP) and were separated by a self-cleaving T2A peptide. This setup allowed for an efficient analysis of the transduction process (Figure 3D). Transduced CFBE maintained CFTR transgene expression for 3-4 weeks and differentiated ciliated cells were present (Fig. 3E). However, the % final transduced cells were reduced from the % seeded transduced cells, indicating a loss of transgene expression over time or a selective pressure against transduced cell

167 survival/proliferation compared to non-transduced cells (Fig. 3F). All downstream functional
168 analyses were measured against the final NHBE percentage in mixed cultures and the final
169 percentage of CFTR-transduced CFBE.
170
171 **CFTR-dependent anion transport is associated with CFTR in NHBE:CFBE co-cultures and**
172 **with K978C-CFTR, but not codon-optimized forms of CFTR in transduced CFBE.**
173 We investigated bioelectric properties of NHBE:CFBE co-cultures and transduced CFBE cells in
174 the presence of CF sputum (Fig. 4A and B). Responses to amiloride, forskolin, $CFTR_{inh}172$ and
175 UTP provided evidence that functional epithelial Na^+ channels (ENaC), CFTR and calcium-
176 activated chloride channels (CaCC) were present. The summarised data from all donors and
177 transductions showed that short circuit current (ΔI_{sc}) in response to $CFTR_{inh}172$ increased in a
178 linear fashion with % of NHBE in the co-culture (R^2=0.91; P<0.0001), and with % CF cell
179 transduction of K978C-CFTR, WT-CFTR and hCAI-CFTRs in transduced CFBE (Slopes -1.56, -
180 0.75 and -0.12, R^2=0.95, 0.93 and 0.57, P<0001, n=8-12 from 3 donors respectively) (Fig. 4C).
181 Regression analysis indicated that 9.8% transduction of K978C-CFTR and 20.4% of WT-CFTR
182 would be sufficient to restore CFTR mediated I_{sc} to that of NHBE in the presence of CF sputum
183 (17 $\mu A/cm^{-2}$) (Fig. 4C). However, 16.7% for K978C-CFTR and 34.7% for WT-CFTR would be
184 required to achieve I_{sc} in NHBE exposed to normal sputum (27.6 $\mu A/cm^{-2}$) (indicative of fully
185 restored function as shown by the dotted lines in Fig. 4C and Fig. S3A). Similar correlations were

observed with basal and forskolin-sensitive I_{sc} (Fig. S4A and C). However, % final transduction with h^K978C-CFTR was poorly correlated with these measurements. Further analysis demonstrated that transduction of K978C-CFTR amplified $CFTR_{inh}172$ ΔI_{sc} >2-fold when compared to WT-CFTR (Fig. 4D). hCAI and h^K978C did not significantly increase $CFTR_{inh}172$ ΔI_{sc} compared to GFP-only transduced CFBE (Fig. 4D). Amiloride-sensitive I_{sc} and UTP stimulated I_{sc} did not correlate with % NHBE (Fig. S3C and E) or % final transduction with any variants of CFTR in CFBE (Fig. S4B and D), suggesting that this effect was specific to CFTR.

The lack of function associated with hCAI-CFTR was counterintuitive considering the increased abundance of membrane localized protein generated in both HEK293T and CFBE cells compared to WT-CFTR. However, there is evidence that overexpression of CFTR can result in basolateral expression of CFTR, reducing transepithelial electrical resistance (TEER) and impeding vectorial ion transport in physiological conditions [11]. Consistent with this hypothesis, transduction with hCAI-CFTR caused a significant decrease in TEER compared to WT-CFTR ($p<0.05$, n=8-12 from 3 CF donors) (Fig. 4E and Fig. S4E). Furthermore, we implemented an artificial basolateral to apical Cl^- gradient in the Ussing chamber to assess if hCAI-CFTR transduced CFBE were able to facilitate Cl^- movement. In the presence of the Cl^- gradient, activation of CFTR by addition of forskolin produced a ΔI_{sc} surpassing that of WT-CFTR (~5.8 fold) and this current was CFTR dependent as it was fully inhibited by $CFTR_{inh}172$ (Fig. 4F).

205

206 **K978C-CFTR more effectively restored ASL hydration in CFBE than WT-CFTR.**

207 A crucial aim of CF therapy is to restore hydration to the CF airway. Therefore, we carried out the
208 well described ASL height assay across the mixed-cultures and transduced CF cells in the presence
209 of CF sputum [26]. As a benchmark for the successful restoration of CFTR function, we once again
210 referred to the results obtained from NHBE cells in the presence of normal lung sputum.
211 ASL height increased with the % transduction of CFBE with either K978C-CFTR or WT-CFTR
212 (1.31±0.53 µm/% final transduced and 0.93±0.50 µm /% final transduced) ($p<0.05$, n=6-8 from 3
213 CF donors respectively) (Figures 5A, 5B, Fig. S5A and Videos S2-6). ASL height did not increase
214 with transduction of codon-optimised forms of CFTR the presence of CF sputum (hCAI:0.17±0.22
215 µm/% final transduced, h^K978C:0.04±0.06 µm/% final transduced). Interestingly, in the presence
216 of CF sputum % NHBE of the co-cultures also had no effect on ASL height:0.08±0.07 µm /%
217 final) (Fig. 5B).

218

219 The change in ASL height was greatest with transduction of K978C-CFTR at ~1.6 fold more than
220 WT-CFTR (Fig. 5C). While we observed a trend towards an increase in ASL height following the
221 stimulation of CFTR with VIP, this increase did not reach statistical significance under any
222 condition when CF sputum was present (see Figure 5D and Figure S5B)[26]. Only NHBE in the

223 presence of normal lung sputum produced a significant increase in ASL height following VIP
224 stimulation (from 8.51±3.27 μm to 16.51±9.41 μm, $p<0.001$; n=9).
225
226 ASL pH levels were restored to physiological levels (7.35) in a similar manner with 13.0% final
227 transduction of K978C-CFTR (n=8 from 3 donors) and 18.7% WT-CFTR (n=11 from 3 donors)
228 (Fig. 5E and Fig. S5C and D) suggesting HCO_3^- secretion through CFTR was also facilitated.
229 Interestingly, hCAI-CFTR and h^K978C-CFTR also appeared to increase ASL pH compared to
230 GFP only transduced CFBE, albeit less effectively than K978C- or WT CFTR.
231
232 **Discussion**
233 The aim of this research was to determine if use of codon optimized or GOF forms of CFTR could
234 improve the efficacy of CF gene therapy in a physiologically relevant airway model that included
235 CF sputum.
236
237 As previously reported, in HEK293T cells, CFTR protein abundance from codon optimised
238 cDNAs was greatly increased compared to WT-CFTR[18]. The replacement of lysine to cysteine in
239 both K978C-CFTR and h^K978C-CFTR decreased protein expression, similar to that reported for
240 G551D/K978C compared to G551D expression in HEK293T cells [21]. The decreased CFTR
241 expression in K978C-CFTR and h^K978C-CFTR may be linked to altered cellular homeostasis

242 due to their enhanced activity, potentially impacting protein synthesis or degradation.
243 Dysregulated ion transport or protein folding can induce cellular stress and alter protein levels [28–
244 30]. Further research is needed to clarify this relationship. The halide transport function of the CFTR
245 variants corelated with protein abundance and the presence of the K978C mutation. K978C is
246 hypothesised to destabilise the inactive state of CFTR and lead to a 2-fold increase in open
247 probability (Po) of the channel[21,31]. Interestingly, pre-treatment of hCAI-CFTR with the CFTR
248 activator VX770 increased activity to the same level as h^K978C-CFTR. VX770 is predicted to
249 induce a conformational change to stabilise the open state of CFTR [23,32] increasing Po of WT-
250 CFTR by ~2 fold [33,34], a phenomenon that we replicated using the HS-YFP quenching assay [35].
251 Thus, our results support that K978C-CFTR produces a similar outcome to that of CFTR
252 potentiation by VX770.
253
254 In CFBE and in the presence of CF sputum, K978C-CFTR was much more effective than other
255 forms of CFTR we studied. K978C-CFTR produced the largest $CFTR_{inh}172$ sensitive $I_{sc,}$ increased
256 ASL height and more effectively restored normal ASL pH than WT-CFTR implying that K978C-
257 CFTR better facilitated Cl^- and HCO_3^- secretion from airway cells. Most notably we show that
258 K978C-CFTR transduction of CFBE in the presence of CF sputum restored ASL heights to those
259 observed in NHBE in the presence of normal lung sputum, a desirable aim for genetic therapy
260 research.

In our study, we used a lentiviral load designed to transduce less than 40% of cells, thereby maximizing the likelihood of single transgene incorporation per transduced cell. This allowed for a more effective comparison of the CFTR variants under consideration in our study. We did not measure mRNA levels thus, variations in transgene expression might exist depending on the site of genomic integration. However, this effect appears to be limited as evidenced by the tight correlation of functional activity with the increase in the percentage of transduced cells.

We provide evidence to support the importance of considering the use of CF sputum in pre-clinical models for CF genetic therapy. In the presence of CF sputum there was a tight linear relationship between $CFTR_{inh}172$-sensitive I_{sc} and % NHBE (endogenous CFTR expression) using the more accurate ddPCR methodology as opposed to initial seeding density. These data contrast to findings where CFTR mediated Cl^- secretion plateaued with ≤50-75% CFTR expression in other mixed culture methods, interpreted as being limited by transporter driven basolateral Cl^- entry [9–11]. We previously showed that the presence of CF sputum compared to normal sputum lowered CFTR-dependent I_{sc} in NHBE cultures [26]. Thus, $CFTR_{inh}172$-sensitive I_{sc} may not be limited by basolateral Cl^- in this circumstance. Our previous work also showed that exposure to CF sputum abrogated hydration of the ASL and responses to VIP compared to normal lung sputum[26]. The lack of change in ASL height with % NHBE suggests that endogenous CFTR function alone may not be sufficient to efficiently rehydrate the ASL in the CF luminal environment.

Our data demonstrates that in the presence of CF sputum, approximately 10% final transduction of cells with K978C-CFTR was sufficient to restore ASL hydration to normal levels (NHBE in the presence of normal sputum). This is approximately half that required for WT-CFTR, in line with the previously reported difference in Po [9]. Full restoration of 'normal function' *in vitro* has been described with <25% transduction of cells with WT-CFTR[12,13]. It is important to highlight, however, that these estimates and interpretation of 'normal' function apply to airway epithelial cells that were not exposed to sputum.

In the context of *in vivo* studies, it is suggested that only 10% of fully functional CFTR transcripts might be enough to prevent development of lung disease[2]. While there are limitations in accurately modelling both endogenous and exogenous CFTR expression *in vitro*, our data suggests a promising potential to acheive desired levels of CFTR function in a CF scenario with K978C-CFTR.

Our evidence indicated that protein expression and localisation of codon optimised CFTR in CFBE was disrupted leading to a lack of vectorial Cl^- transport. FRAP can be used to determine the rates of local protein turnover, identify mobile fractions, and demonstrate exchange between cellular compartments or lack thereof in live cells[36]. In this assay, h^K978C-CFTR displayed free, rapid diffusion, providing evidence that the protein was not membrane bound. hCAI-CFTR was present

in a membrane-associated state, but likely mislocalised as evidenced by a reduction in TEER and the requirement of an artificial Cl^- gradient to demonstrate function. Such overexpression of CFTR was shown to perturb polarisation of epithelial cells, localisation of membrane proteins and membrane potential, all of which compromise vectorial Cl^- transport [37,38]. For example, CFTR under control of a CMV promoter generated basolateral CFTR[11]. Furthermore, codon optimisation can affect subsequent mRNA secondary structure, co-translational protein folding and interaction with noncoding RNAs which are involved in regulation of CFTR gene expression, none of which were explored in this study [39–41]. Interestingly, the codon optimised variants of CFTR did restore ASL pH but at higher % cellular transduction rates than WT or K978C, a phenomenon also captured in other work[19]. Explanations for this include increased paracellular basolateral to apical movement of HCO_3^-, due to decreased TEER or increased HCO_3^- secretion via other channels that interact with CFTR, for example, SLC26 transporters[19,42]. The exclusive use of a high activity viral SSFV promoter is a notable constraint of our study. As a result, further investigation is required to discern whether the use of lower activity promoters, that are translatable to *in vivo* study, might improve the ability of hCAI-CFTR and h^K978C-CFTR to restore critical epithelial characteristics in CFBE cells. These include the phosphoglycerate kinase (PGK) and elongation factor 1α (EF1α) promoters, both of which have been employed to drive the expression of codon-optimized CFTR in CFBE with some success[19].

While this study provided evidence of CFTR expression in transduced cells (Figure 3E), we did not focus on which cell-types expressed the CFTRs. Lentiviral transduction does not impede the differentiation of airway progenitor cells, and all differentiated airway cell types are capable of expressing the introduced transgene[43]. Cilliated and secretory cells are the most numerous cells in NHBE/CFBE. Ionocytes are rare (0.5-1.0%) but express the highest levels of CFTR although the relative contribution of each cell type to epithelial anion transport is still under debate [44]t[45–47]. Given the cellular transduction efficiencies we observed, functional restoration is likely driven by cell types other than ionocytes. How individual cell transduction modifies CFTR function is a compelling direction for future research to refine genetic therapy strategies for CF.

In conclusion, we have provided proof of principle that GOF variant K978C-CFTR was more effective at restoring anion secretion, ASL hydration and pH to CFBE than WT-CFTR. However, we found that increasing CFTR protein using codon optimisation did not translate to better function in CFBE. Importantly, K987C-CFTR was able to restore function to CFBE even in the presence of CF sputum. These data provide proof of principle that GOF variants may be more effective than codon optimised forms of CFTR for CF gene therapy.

Materials and Methods

Primary Human Bronchial Epithelial Cell Culture

CFBE and non-CF primary human bronchial epithelial cells (NHBE) were obtained with ethical approval from the University of North Carolina at Chapel Hill Biomedical Review Board (protocol #03 1396). Cells were cultured on permeable supports and maintained at air-liquid interface (ALI) in a modified bronchial epithelial growth medium for 21-28 days [48]. Co-cultures were generated by mixing NHBE and CFBE of different sex (XX or XY) at 10%, 25%, 50% and 75% (non-CF:CF). Cultures were incubated with 20 µl apically applied CF sputum 4 hrs prior to functional experimentation as described [26]. Donor demographics are provided in Table S1. BMI-1 transduced Cystic fibrosis (F508del/F508del) bronchial epithelial cells (CFBE BMI-1) were generously supplied by Professor Stephen Hart (UCL, Institute of Child Health) [27].

Sputum preparation

Airway sputum samples were obtained as described in University of North Carolina protocol[49]. An ultrasonic nebuliser was filled with 30 ml of 5% hypertonic saline for a 12-min inhalation period. After the 12-min inhalation period subjects underwent a cleansing procedure: gargle and rinse the mouth with water, scrape and clear the back of the throat (to avoid the inclusion of non-airway fluid samples) and blow nose. The subjects were asked to deliver a chesty cough and expectorated the secretions into a sterile specimen jar. This was capped and placed on ice and

354 stored at -80ºC. Donor demographics of induced sputum donors are provided in Table S2 and are
355 reported in Woodall et al., 2021.
356
357 For each experiment un-refined sputum samples were thawed on ice and centrifuged at 4000 x g
358 for 20 minutes to remove cells, bacteria and macromolecules. The supernatants were pooled for
359 all downstream experimentation.
360
361 **Droplet Digital PCR**
362 ddPCR using primers for amelogenin-X isoform (AMELX) and amelogenin- Y isoform (AMELY)
363 and probes with FAM and VIC reporters, respectively (AB-Bioscience, UK), were performed as
364 previously described [50]. Primer sequences are provided in Table S6. FAM and VIC positive (+ve)
365 droplets from each well of the PCR plate were measured and analysed using associated software
366 QuantaSoft. These data are presented normalised with exclusively male cultures (n=10) set at 0%
367 and female (n=10) set at 100%.
368
369 **Immunohistochemistry**
370 ALI cultures were fixed in 4% PFA, permeabilized (0.1% Triton X-100 in PBS) and blocked with
371 blocking buffer (Table S5), prior to overnight incubation at 4°C with primary antisera (α-tubulin,
372 GFP) followed by visualization with Alexa Fluor 568 or Alexa Fluor 488. Membranes were

373 counterstained with phalloidin (4 µg/mL) and DAPI (2 µg/mL) for 30 minutes at room
374 temperature. Images were captured using a Leica SP8 confocal microscope with LAS AF (Leica)
375 acquisition software (antisera and fluorophore dilutions and catalogue numbers: Table S3, S4).
376
377 **Electrophysiological measurement**
378 Transepithelial ion transport was measured using the Ussing chamber technique using symmetrical
379 buffers (Table S5) and the following drugs: amiloride (apical, 100 µM) to inhibit the epithelial
380 sodium channel (ENaC); forskolin (bilaterally, 10 µM) to stimulate CFTR; $CFTR_{inh}172$ (apical,
381 10 µM) to inhibit CFTR; and UTP (apical, 100 µM) to stimulate calcium-activated chloride
382 channels, as previously described[26]. For Cl^- gradient studies the apical chamber was replaced with
383 Cl^- free Ussing Buffer (Table S5). Data were analysed using Acquire and Analysis (version 1.2)
384 software (Physiologic Instruments). All drugs/chemicals were obtained from Sigma-Aldrich.
385
386 **Airway surface liquid (ASL) height /pH measurements**
387 ASL exposed to CF sputum (CFS) or normal lung sputum (normal lung sputum, 20 µl) were
388 labelled with 0.5 mg/ml of 10 kDa dextran-tetramethylrhodamine (Life Technologies, USA).
389 Images were obtained before and 60 minutes after addition of basolateral VIP (100nM) to induce
390 CFTR mediated secretion by using a Leica SP8 confocal microscope with a ×63/1.3 numerical
391 aperture (NA) glycerol immersion lens in XZ-scanning mode as described [26,51]. ASL pH was

392 measured using Alexa 647 dextran (10 μM) and pH-sensitive pHrodo red dextran (10 μM) in 20
393 μl CF sputum. After 60-minute incubation at 37 °C in air + 5% CO_2 excitation/emission at
394 562/592nm and 650/668nm was measured. Apical pH was calculated as the fluorescence ratio
395 pHrodo red dextran: Alexa 647 dextran less background fluorescence from non-labelled ASL and
396 results aligned to a standard curve generated from controls of known pH 6.0-7.5) as described by
397 [52].
398
399 **CFTR codon optimisation**
400 The WT-CFTR construct, generously supplied by Stephen Hart, contained the native codons
401 derived from a cDNA clone (GenBank, M28668.1) encoding human CFTR. The Codon optimized
402 versions of CFTR were generously supplied by David Mueller, in which the codons were nearly
403 entirely derived using codons with high codon adaptation index[53] (CAI) values (from www.jcat.de)
404 and named hCAI by the laboratory team that designed it (Department of Biochemistry and
405 Molecular Biology, Rosalind Franklin University)[18].
406
407 **Site-directed mutagenesis**
408 Primers containing the nucleotide sequence to alter WT CFTR with the K978C mutation (K978C),
409 hCAI with the K978C mutation (h^K978C) or for T2A mutagenesis were designed using
410 SnapGene software (Table S6) and synthesised by Sigma Aldrich.

411 Site directed mutagenesis was carried out on an Eppendorf® Mastercycler® Pro Thermal Cycler
412 using PhusionTM Hot Start II High-Fidelity PCR Master Mix, following manufacturer's protocol.
413 The PCR amplified DNA products were confirmed by sequencing
414 (GENEWIZ®,https://www.genewiz.com).
415
416 **Lentivirus construction and cell transduction**
417 Second generation lentiviral transfer constructs containing the SFFV promoter upstream of GFP
418 and CFTR. In some constructs, the transgene was separated by a self-cleaving T2A peptide. The
419 construct, packaging plasmid (pMD2.G) and envelop plasmid (pCMVR8.74) were packaged into
420 HEK293T cells via co-transfection with lipofectamine 2000 (Thermofisher) [54]. The day before
421 transduction, 2.5 x 10^5 target cells were seeded onto a collagen coated 6-well plate. Opti-MEM™
422 supplemented with 8 μg polybrene was mixed with desired volume of harvested lentivirus per well.
423 For viral titre definition, volumes of either 10 μl, 5 μl, 2.5 μl and 1.25 μl of lentiviral suspension
424 were added to this mix. Cells were washed 1x with PBS prior to addition of the transduction
425 mixture. Cells were incubated for 6 hours after which the transduction mix was aspirated and
426 replaced with 2 ml of growth media. Viral titre was measured by quantifying GFP positive cells
427 with flow cytometry on an Attune NxT 2 and analysed with FlowJo software.
428

Following the methodology suggested by Charrier et al., 2011[55] we employed viral suspensions that transduced fewer than 40% of CFBE cells from each donor (MOI <0.4). This approach was chosen to ensure the integration of a single vector copy per cell, translating to the incorporation of one transgene per cell.

Titre and quantification of transduction efficiency

For definition of the final % of cells expressing the transgene (% final transduced), cultures were analysed 4 hours prior to functional assays. Cultures were first washed 3x with PBS to remove residual phenol red in growth medium and submerged in Ussing buffer for duration of microscopy analysis. At least 10 images were taken from each well with a Cytation™ 5 - Cell Imaging Multi-Mode Reader at 4x magnification.

Both fluorescent signal and transmitted light were taken for each well. Images were subject to analysis on Image-J with a macro designed specifically for the purpose of quantifying the fluorescent:non-fluorescent cell percentage. The macro converted transmitted light images and fluorescence images from the same XY position to binary masks and allowed for accurate identification of fluorescent signal and non-fluorescent cells. Dead cells were discarded by a size and granulation threshold. Transduction efficiency was calculated with the following equation, where n is the number of images taken per well:

$$\% \text{ Final} = \sum \left(\frac{(\text{GFP positive pixels})}{(\text{GFP positive pixels}) + (\text{total pixels within all cell regions})} \right) \div (0.01n)$$

The results produced from this method were initially verified by flow cytometry analysis of a 1.5 x 10^5 cell sample from their respective wells.

Halide-sensitive yellow fluorescent protein quenching assay

HEK293T cells were transfected with 100ng pcDNA3.1_YFP-H148Q/I152L (HS-YFP) [56] and CFTR cDNAs (WT, K978C, hCAI and h^K978C) (Fig. 2A) using lipofectamine (Thermofisher). At 24 hours post transfection, the medium was replaced with 100 µl Standard buffer (Table S5). HS-YFP fluorescence inside the cells was measured using ImageXpress as described in [57], with a 20× objective, and 472/520 nm excitation / emission filters at 28ºC. Images were acquired every 2 seconds for 150 seconds. At 20 seconds I^- in standard buffer was automatically dispensed into the extracellular medium so that the final concentration of I^- in the extracellular medium was 100 mM. At 40 seconds, forskolin was added at a final concentration of 10 µM while keeping the concentrations of the other components unchanged. Images were analysed using ImageJ (http://rsbweb.nih.gov/ij/). Iodide binding to HS-YFP decreases fluorescence (F), thus F/F_{max} (f) is used to quantify I^- entry, where the concentration of iodide inside the cells was defined as $[I^-]_{in} = K_I ((1-f) / f)$ [35,57,58]. The binding affinity of I^- to HS-YFP, K_I, was set to 1.9 mM [35,56–58]. CFTR activity was quantified as the maximal rate of I^- entry into cells (mM/s)[57,59]

466

467 **Western blot**

468 Cells were lysed in NP-40 Lysis Buffer (Table S5), incubated on ice for 20 minutes then
469 centrifuged at 15,000g for 20 minutes. Protein concentration was determined by Pierce™ BCA
470 Protein Assay Kit and 20 µg protein was denatured with 2.5 µl LDS sample buffer and 1 µl
471 reducing agent (NuPAGE) a at 37°C for 30 minutes. Samples were resolved on NuPAGE 4-12%
472 Bis-Tris Protein Gels with mass standards 10-250 kDa (LI-COR). Proteins were transferred to
473 Immobilon®-FL PVDF membrane (Millipore). Membranes were blocked in Odyssey® Blocking
474 Buffer (LI-COR), immunostained with anti-CFTR or anti-α Tubulin followed by IRDye® 800CW
475 Goat anti-Mouse IgG (LI-COR), visualised and quantified on an Odyssey IR imager (LI-COR)
476 (Tables S3 and S4)

477

478 **Fluorescence recovery after photobleaching**

479 GFP linked CFTR transduced CFBE BMI-1 were imaged on a Leica SP5 inverted confocal
480 microscope 63X/1.3 glycerol as described [60]. Regions of interest (ROIs) of 20 pixels were selected
481 as the point of highest fluorescence of individual cells. The mean fluorescence of 3 scan iterations
482 (~1 second per iteration) were acquired. ROIs were using 100% transmission of the 488-nm-
483 wavelength laser and fluorescence recovery after photobleaching (FRAP) was measured for ~70
484 scan iterations. The fluorescence values were normalised to the initial pre-bleach value (1) and the

485 value immediately post-bleach (0). The Mobile Fraction (M_f) was calculated using the equation:

486 $$M_f = \left(\frac{F_{end}-F_{post}}{F_{pre}-F_{post}}\right)$$

487 Pre-FRAP images were used to obtain mean fluorescence values from the intracellular region of
488 the cell. At least 10 regions of interest (ROI) were measured for each cell. Ratio of mean
489 intracellular to mean peripheral (2.5 µm from and including the most distal point of fluorescence
490 of each cell) fluorescence (RFU) were obtained using NIS-Elements software (Figure S2C).

491

492 **Statistics**

493 Normally distributed data were analysed using ANOVA followed by Tukey's test or unpaired t-
494 test with Welch's correction. Paired t tests were applied to samples from the same donor but subject
495 to different treatments. Non-parametric equivalents (Mann–Whitney test, Kruskal–Wallis test with
496 Dunn's multiple comparisons test) were used when data were not normally distributed. Data are
497 shown as individual points and/or mean ± standard deviation. For linear regression, the coefficient
498 of determination (R^2) and whether the slope significantly differed from zero are presented. ns: no
499 significant difference. Significant differences are indicated with *: $p<0.05$; **: $p<0.01$; ***:
500 $p<0.001$. Data analyses were performed using GraphPad Prism v9.1.0 (GraphPad Software).

501

502 **Acknowledgements**

Funded by the Cystic Fibrosis Trust Project No: SRC 006. Provision of cells and media was supported by TARRAN17GO from the Cystic Fibrosis Foundation, BOUCHE15RO from the Cystic Fibrosis Foundation and P30 DK065988 from the NIH, USA.

We thank the CF SRC team for advice and input. Particularly, Ileana Guerrini (ICH) for help in developing the lentiviral constructs. We thank Emily Langron (UCL) for advice and direction with the halide sensitive YFP assay. We thank Wei Wang (UAB) for sharing their knowledge on K978C CFTR. We thank the University of North Carolina (UNC) Cystic Fibrosis Center Tissue Core (Director: Scott Randell) for providing cells, media and expert advice. In addition, we thank Rhianna Lee, Michael Chua, Lolita Radet, Saira Ahmad, Patrick Moore, Megan Webster, Ozge Beyazcicek, Eric Scott and Maria Sassano for their help and support at UNC. BioRender.com was used to create images included in this manuscript.

Keywords

Cystic fibrosis, gene therapy, CFTR, airway epithelium

Author Contributions

DB and MW conceived the idea. MW and HA carried out the experimental work. RT and RL provided resources and supervised MW. SP, PV and JC provided resources and helped perform

assays. DB/SH supervised MW and edited manuscript. DB and MW carried out analyses, wrote and edited the manuscript.

Declaration of Interests

The authors have no conflicts of interests to declare

Data Availability Statement

The experimental data that support the findings of this study are available in Figshare with the identifiers https://doi.org/10.6084/m9.figshare.23915565.v1, https://doi.org/10.6084/m9.figshare.23907711.v1, https://doi.org/10.6084/m9.figshare.23907726.v1. Additional image sets are available on request from the corresponding author.

References

1. Wilschanski, M. (2012). Class 1 CF mutations. Front Pharmacol *3 JUN*. 10.3389/fphar.2012.00117.

2. Chu, C.S., Trapnell, B.C., Curristin, S.M., Cutting, G.R., and Crystal, R.G. (1992). Extensive posttranscriptional deletion of the coding sequences for part of nucleotide-binding fold 1 in respiratory epithelial mRNA transcripts of the cystic fibrosis transmembrane conductance regulator gene is not associated with the clinical manifestations of cystic fibrosis. J Clin Invest *90*, 785–790.

3. Char, J.E., Wolfe, M.H., Cho, H.J., Park, I.H., Jeong, J.H., Frisbee, E., Dunn, C., Davies, Z., Milla, C., Moss, R.B., et al. (2014). A little CFTR goes a long way: CFTR-dependent sweat secretion from G551D and R117H-5T cystic fibrosis subjects taking ivacaftor. PLoS One *9*. 10.1371/journal.pone.0088564.

4. Cooney, A.L., Abou Alaiwa, M.H., Shah, V.S., Bouzek, D.C., Stroik, M.R., Powers, L.S., Gansemer, N.D., Meyerholz, D.K., Welsh, M.J., Stoltz, D.A., et al. (2016). Lentiviral-mediated phenotypic correction of cystic fibrosis pigs. JCI Insight, Sep 8;1(14):e88730.

5. Maule, G., Arosio, D., and Cereseto, A. (2020). Gene Therapy for Cystic Fibrosis: Progress and Challenges of Genome Editing. Int J Mol Sci *21*, 1–13.

6. Ramalho, A.S., Beck, S., Meyer, M., Penque, D., Cutting, G.R., and Amaral, M.D. (2002). Five Percent of Normal Cystic Fibrosis Transmembrane Conductance

Regulator mRNA Ameliorates the Severity of Pulmonary Disease in Cystic Fibrosis. Am J Respir Cell Mol Biol, *5*, 619-27.

7. King, N.E., Suzuki, S., Barillà, C., Hawkins, F.J., Randell, S.H., Reynolds, S.D., Stripp, B.R., and Davis, B.R. (2020). Correction of Airway Stem Cells: Genome Editing Approaches for the Treatment of Cystic Fibrosis. Hum Gene Ther *31*, 956-972.

8. Cooney, A.L., McCray, P.B., and Sinn, P.L. (2018). Cystic Fibrosis Gene Therapy: Looking Back, Looking Forward. Genes (Basel) *9*. 538.

9. Shah, V.S., Ernst, S., Tang, X.X., Karp, P.H., Parker, C.P., Ostedgaard, L.S., and Welsh, M.J. (2016). Relationships among CFTR expression, HCO3- secretion, and host defense may inform gene- and cell-based cystic fibrosis therapies. Proc Natl Acad Sci U S A *113*, 5382–5387.

10. Dannhoffer, L., Blouquit-Laye, S., Regnier, A., and Chinet, T. (2009). Functional Properties of Mixed Cystic Fibrosis and Normal Bronchial Epithelial Cell Cultures. Am J Respir Cell Mol Biol *40*, 717–723.

11. Farmen, S.L., Karp, P.H., Ng, P., Palmer, D.J., Koehler, D.R., Hu, J., Beaudet, A.L., Zabner, J., and Welsh, M.J. (2005). Gene transfer of CFTR to airway epithelia: low levels of expression are sufficient to correct Cl^- transport and overexpression can generate basolateral CFTR. American Journal of Physiology-Lung Cellular and Molecular Physiology *289*, L1123–L1130.

12. Johnson, L.G., Olsen, J.C., Sarkadi, B., Moore, K.L., Swanstrom, R., and Boucher, R.C. (1992). Efficiency of gene transfer for restoration of normal airway epithelial function in cystic fibrosis. Nat Genet *2*, 21–25.

13. Zhang, L., Button, B., Gabriel, S.E., Burkett, S., Yan, Y., Skiadopoulos, M.H., Dang, Y.L., Vogel, L.N., McKay, T., Mengos, A., et al. (2009). CFTR delivery to 25% of surface epithelial cells restores normal rates of mucus transport to human cystic fibrosis airway epithelium. PLoS Biol *7*, e1000155. 10.

14. Alton, E.W.F.W., Armstrong, D.K., Ashby, D., Bayfield, K.J., Bilton, D., Bloomfield, E. v, Boyd, A.C., Brand, J., Buchan, R., Calcedo, R., et al. (2015). Repeated nebulisation of non-viral CFTR gene therapy in patients with cystic fibrosis: a randomised, double-blind, placebo-controlled, phase 2b trial. Lancet Respir Med *3*, 684–691.

15. Padegimas, L., Kowalczyk, T.H., Adams, S., Gedeon, C.R., Oette, S.M., Dines, K., Hyatt, S.L., Sesenoglu-Laird, O., Tyr, O., Moen, R.C., et al. (2012). Optimization of hCFTR lung expression in mice using DNA nanoparticles. Molecular Therapy *20*, 63–72.

16. Yew, N.S., Wang, K.X., Przybylska, M., Bagley, R.G., Stedman, M., Marshall, J., Scheule, R.K., and Cheng, S.H. (1999). Contribution of plasmid DNA to inflammation in the lung after administration of cationic lipid:pDNA complexes. Hum Gene Ther *10*, 223–234.

17. Bartoszewski, R., Króliczewski, J., Piotrowski, A., Jasiecka, A.J., Bartoszewska, S., Vecchio-Pagan, B., Fu, L., Sobolewska, A., Matalon, S., Cutting, G.R., et al. (2016). Codon

bias and the folding dynamics of the cystic fibrosis transmembrane conductance regulator. Cell Mol Biol Lett *21*, 23.

18. Shah, K., Cheng, Y., Hahn, B., Bridges, R., Bradbury, N.A., and Mueller, D.M. (2015). Synonymous codon usage affects the expression of wild type and F508del CFTR. J Mol Biol *427*, 1464–1479.

19. Marquez Loza, L.I., Cooney, A.L., Dong, Q., Randak, C.O., Rivella, S., Sinn, P.L., and McCray, P.B. (2021). Increased CFTR expression and function from an optimized lentiviral vector for cystic fibrosis gene therapy. Mol Ther Methods Clin Dev *21*, 94–106.

20. Linsdell, P. (2016). Anion conductance selectivity mechanism of the CFTR chloride channel. Biochim Biophys Acta Biomembr *1858*, 740–747.

21. Wang, W., Wu, J., Bernard, K., Li, G., Wang, G., Bevensee, M.O., and Kirk, K.L. (2010). ATP-independent CFTR channel gating and allosteric modulation by phosphorylation. Proc Natl Acad Sci U S A *107*, 3888–3893.

22. Jih, K.Y., and Hwang, T.C. (2013). Vx-770 potentiates CFTR function by promoting decoupling between the gating cycle and ATP hydrolysis cycle. Proc Natl Acad Sci U S A *110*, 4404–4409.

23. Yeh, H.I., Qiu, L., Sohma, Y., Conrath, K., Zou, X., and Hwang, T.C. (2019). Identifying the molecular target sites for CFTR potentiators GLPG1837 and VX-770. J Gen Physiol *151*, 912–928.

24. Woodall, M.N.J., Masonou, T., Case, K.M., and Smith, C.M. (2021). Human models for COVID-19 research. J Physiol *599*, 4255–4267.

25. Awatade, N.T., Wong, S.L., Hewson, C.K., Fawcett, L.K., Kicic, A., Jaffe, A., and Waters, S.A. (2018). Human Primary Epithelial Cell Models: Promising Tools in the Era of Cystic Fibrosis Personalized Medicine. Front Pharmacol *9*, 1429.

26. Woodall, M., Reidel, B., Kesimer, M., Tarran, R., and Baines, D.L. (2021). Culture with apically applied healthy or disease sputum alters the airway surface liquid proteome and ion transport across human bronchial epithelial cells. Am J Physiol Cell Physiol *321*, C954–C963.

27. Munye, M.M., Shoemark, A., Hirst, R.A., Delhove, J.M., Sharp, T. V., McKay, T.R., O'Callaghan, C., Baines, D.L., Howe, S.J., and Hart, S.L. (2017). BMI-1 extends proliferative potential of human bronchial epithelial cells while retaining their mucociliary differentiation capacity. American Journal of Physiology-Lung Cellular and Molecular Physiology *312*, L258–L267..

28. Charras, G.T. (2008). A short history of blebbing. J Microsc *231*, 466–478.

29. Rutkowski, D.T., and Kaufman, R.J. (2004). A trip to the ER: Coping with stress. Trends Cell Biol *14*, 20–28.

30. Miura, G. (2014). Death by ions. Nature Chemical Biology 2014 10:10 *10*, 795–795.

31. Wang, W., Roessler, B.C., and Kirk, K.L. (2014). An electrostatic interaction at the tetrahelix bundle promotes phosphorylation-dependent cystic fibrosis transmembrane conductance regulator (CFTR) channel opening. Journal of Biological Chemistry *289*, 30364–30378.

32. Langron, E., Prins, S., and Vergani, P. (2018). Potentiation of the cystic fibrosis transmembrane conductance regulator by VX-770 involves stabilization of the pre-hydro. Br J Pharmacol *175*, 3990–4002.

33. van Goor, F., Hadida, S., Grootenhuis, P.D.J., Burton, B., Cao, D., Neuberger, T., Turnbull, A., Singh, A., Joubran, J., Hazlewood, A., et al. (2009). Rescue of CF airway epithelial cell function in vitro by a CFTR potentiator, VX-770. Proc Natl Acad Sci U S A *106*, 18825–18830.

34. Yu, H., Burton, B., Huang, C.J., Worley, J., Cao, D., Johnson, J.P., Urrutia, A., Joubran, J., Seepersaud, S., Sussky, K., et al. (2012). Ivacaftor potentiation of multiple CFTR channels with gating mutations. Journal of Cystic Fibrosis *11*, 237–245.

35. Galietta, L.J.V., Springsteel, M.F., Eda, M., Niedzinski, E.J., By, K., Haddadin, M.J., Kurth, M.J., Nantz, M.H., and Verkman, A.S. (2001). Novel CFTR chloride channel activators identified by screening of combinatorial libraries based on flavone and benzoquinolizinium lead compounds. J Biol Chem *276*, 19723–19728.

646 36. Bancaud, A., Huet, S., Rabut, G., and Ellenberg, J. (2010). Fluorescence perturbation
647 techniques to study mobility and molecular dynamics of proteins in live cells: FRAP,
648 Photoactivation, Photoconversion, and FLIP. Cold Spring Harb Protoc Dec 1, *12*.
649 10.1101/pdb.top90.
650 37. Mohammad-Panah, R., Demolombe, S., Riochet, D., Leblais, V., Loussouarn, G., Pollard,
651 H., Baró, I., and Escande, D. (1998). Hyperexpression of recombinant CFTR in
652 heterologous cells alters its physiological properties. Am J Physiol *274*, C310-C318.
653 38. Ye, L., Chan, S., Chow, Y.-H., Tsui, L.-C., and Hu, J. (2001). Regulated Expression of the
654 Human CFTR Gene in Epithelial Cells. Molecular Therapy *3*, 723–733.
655 39. Mauro, V.P. (2018). Codon Optimization in the Production of Recombinant
656 Biotherapeutics: Potential Risks and Considerations. BioDrugs 2018 32:1 *32*, 69–81.
657 40. Glasgow, A.M.A., de Santi, C., and Greene, C.M. (2018). Non-coding RNA in cystic
658 fibrosis. Biochem Soc Trans *46*, 619–630.
659 41. Kim, S.J., Yoon, J.S., Shishido, H., Yang, Z., Rooney, L.A.A., Barral, J.M., and Skach,
660 W.R. (2015). Translational tuning optimizes nascent protein folding in cells. Science (1979)
661 *348*, 444–448.
662 42. Garnett, J.P., Hickman, E., Burrows, R., Hegyi, P., Tiszlavicz, L., Cuthbert, A.W., Fong,
663 P., and Gray, M.A. (2011). Novel role for pendrin in orchestrating bicarbonate secretion in

cystic fibrosis transmembrane conductance regulator (CFTR)-expressing airway serous cells. Journal of Biological Chemistry *286*, 41069–41082.

43. Cooney, A.L., Thurman, A.L., McCray, P.B., Pezzulo, A.A., and Sinn, P.L. (2021). Lentiviral vectors transduce lung stem cells without disrupting plasticity. Mol Ther Nucleic Acids *25*, 293–301.

44. Montoro, D.T., Haber, A.L., Biton, M., Vinarsky, V., Lin, B., Birket, S.E., Yuan, F., Chen, S., Leung, H.M., Villoria, J., et al. (2018). A revised airway epithelial hierarchy includes CFTR-expressing ionocytes. Nature *560*, 319–324.

45. Scudieri, P., Musante, I., Venturini, A., Guidone, D., Genovese, M., Cresta, F., Caci, E., Palleschi, A., Poeta, M., Santamaria, F., et al. (2020). Ionocytes and CFTR Chloride Channel Expression in Normal and Cystic Fibrosis Nasal and Bronchial Epithelial Cells. Cells *9*, 2090.

46. Plasschaert, L.W., Žilionis, R., Choo-Wing, R., Savova, V., Knehr, J., Roma, G., Klein, A.M., and Jaffe, A.B. (2018). A single cell atlas of the tracheal epithelium reveals the CFTR-rich pulmonary ionocyte. Nature *560*, 377-381.

47. Sato, Y., Kim, D., Turner, M.J., Luo, Y., Zaidi, S.S.Z., Thomas, D.Y., and Hanrahan, J.W. (2023). Ionocyte-Specific Regulation of CFTR. Mar 23. doi: 10.1165/rcmb.2022-0241OC. Online ahead of print.

48. Fulcher, M.L., and Randell, S.H. (2013). Human Nasal and Tracheo-Bronchial Respiratory Epithelial Cell Culture. Methods Mol Biol. *945*,109-21

49. Alexis, N.E., Hu, S.C., Zeman, K., Alter, T., and Bennett, W.D. (2001). Induced sputum derives from the central airways: Confirmation using a radiolabeled aerosol bolus delivery technique. Am J Respir Crit Care Med *164*, 1964–1970.

50. George, D., Czech, J., John, B., Yu, M., and Jennings, L.J. (2013). Detection and quantification of chimerism by droplet digital PCR. Chimerism *4*, 102–108.

51. Choi, H.-C., Kim, C.S.K., and Tarran, R. (2015). Automated acquisition and analysis of airway surface liquid height by confocal microscopy. American Journal of Physiology-Lung Cellular and Molecular Physiology *309*, L109–L118.

52. Garland, A.L., Walton, W.G., Coakley, R.D., Tan, C.D., Gilmore, R.C., Hobbs, C.A., Tripathy, A., Clunes, L.A., Bencharit, S., Stutts, M.J., et al. (2013). Molecular basis for pH-dependent mucosal dehydration in cystic fibrosis airways. Proc Natl Acad Sci U S A *110*, 15973–15978.

53. Grote, A., Hiller, K., Scheer, M., Münch, R., Nörtemann, B., Hempel, D.C., and Jahn, D. (2005). JCat: a novel tool to adapt codon usage of a target gene to its potential expression host. Nucleic Acids Res *33*, W526–W531.

54. Vink, C.A., Counsell, J.R., Perocheau, D.P., Karda, R., Buckley, S.M.K., Brugman, M.H., Galla, M., Schambach, A., McKay, T.R., Waddington, S.N., et al. (2017). Eliminating HIV-1 Packaging Sequences from Lentiviral Vector Proviruses Enhances Safety and Expedites Gene Transfer for Gene Therapy. Mol Ther *25*, 1790–1804.

55. Charrier, S., Ferrand, M., Zerbato, M., Précigout, G., Viornery, A., Bucher-Laurent, S., Benkhelifa-Ziyyat, S., Merten, O.W., Perea, J., and Galy, A. (2011). Quantification of lentiviral vector copy numbers in individual hematopoietic colony-forming cells shows vector dose-dependent effects on the frequency and level of transduction. Gene Ther *18*, 479–487.

56. Galietta, L.J.V., Haggie, P.M., and Verkman, A.S. (2001). Green fluorescent protein-based halide indicators with improved chloride and iodide affinities. FEBS Lett *499*, 220–224.

57. Langron, E., Simone, M.I., Delalande, C.M.S., Reymond, J.L., Selwood, D.L., and Vergani, P. (2017). Improved fluorescence assays to measure the defects associated with F508del-CFTR allow identification of new active compounds. Br J Pharmacol *174*, 525–539.

58. Prins, S., Langron, E., Hastings, C., Hill, E.J., Stefan, A.C., Griffin, L.D., and Vergani, P. (2020). Fluorescence assay for simultaneous quantification of CFTR ion-channel function and plasma membrane proximity. J Biol Chem *295*, 16529–16544.

59. Pedemonte, N., Zegarra-Moran, O., and Galietta, L.J.V. (2011). High-throughput screening of libraries of compounds to identify CFTR modulators. Methods Mol Biol *741*, 13–21.

60. Woodall, M., Jacob, J., Kalsi, K.K., Schroeder, V., Davis, E., Kenyon, B., Khan, I., Garnett, J.P., Tarran, R., and Baines, D.L. (2020). E-cigarette constituents propylene glycol and vegetable glycerin decrease glucose uptake and its metabolism in airway epithelial cells in vitro. Am J Physiol Lung Cell Mol Physiol *319*, L957–L967.

722

723

724 **Figure legends**

725 **Figure 1. Impact of CFTR cDNAs on protein production and function in transfected**
726 **HEK293T cells.** (A)(i) Illustrations representing each CFTR variant: wild type (blue), K978C
727 mutation (purple), high codon adaptation index CFTR (cyan; hCAI), and hCAI carrying the K978C
728 mutation (pink; h^K978C). (A)(ii) Schematic representation of halide-sensitive YFP (HS-YFP)
729 quenching assay: HEK293T cells co-transfected with HS-YFP and CFTR variants. CFTR
730 activators induce facilitated anion movement through CFTR channels, leading to HS-YFP
731 fluorescence quenching. (B) Western blot of protein extracts from HEK293T cells co-transfected
732 with HS-YFP and CFTR cDNAs. CFTR bands C and B (green) and HS-YFP (red) are indicated.
733 Molecular weight markers (red) are displayed on the left side of the blot. (C) Quantification of
734 CFTR protein abundance, expressed as the mean of (CFTR (bands C + B)/ HS-YFP) normalized
735 to WT for standardization between blots. Data are represented as mean ± SD. Differences were
736 compared by one-way ANOVA followed by Tukey's post hoc tests. Significantly different *:
737 $p<0.05$; **: $p<0.01$; n=3. (D) HS-YFP fluorescence quenching over time in HEK293 cells
738 transfected with HS-YFP alone or co-transfected with CFTR cDNAs under different conditions:
739 DMSO (vehicle) (D), Forskolin (FSK) (E), and FSK plus the CFTR potentiator VX770
740 (FSK+VX770) (F), all added at timepoint 0. The maximal rate of I^- influx ($\Delta[I^-]/\Delta t$) is

741 summarized for CFTR cDNA and conditions in (G). Data are represented as mean ± SD along
742 with individual data points. CFTR function was compared by two-way ANOVA followed by
743 Tukey's post hoc tests. Significantly different *: $p<0.05$; **: $p<0.01$; ***: $p<0.001$, n=3.
744
745 **Figure 2. CFTR protein expression and localization in CFBE.** (A) Representative western blot
746 of soluble protein fraction from differentiated CFBE cultures transduced with CFTR cDNAs or
747 GFP alone (as labeled). Blots are probed with anti-CFTR (CFTR 596) and anti-GFP. CFTR bands
748 C and B (green), GFP (red), and molecular weight markers (red) are displayed. (B) Summary of
749 the relative fluorescence units (RFU) for CFTR bands C and B in relation to the % final
750 transduction, normalized to WT for each CFTR cDNA. Data are shown as mean ± SD with
751 individual data points (n=4-7 from 3 donors). Treatments were compared by two-way ANOVA
752 with Tukey's post hoc analyses; Significantly different **: $p<0.01$; ***: $p<0.001$. RFU ratio of
753 bands B:C are displayed below the graph. (C) Representative confocal live images (x60, excitation
754 488 nm/emission 507 nm) of CFBE BMI-1 cells transduced with GFP linked to CFTR cDNAs or
755 GFP alone. Cell blebbing is indicated with white arrows, with a 50 μm scale bar displayed. (D)
756 Schematic detailing FRAP protocol, indicating stages of Pre-bleach, Post-bleach, and End within
757 the region of interest (ROI), represented by the white square. (E) Kinetic plot showcasing
758 fluorescence (F) change over time within an ROI on the cell periphery. The bleach point is marked
759 with an arrow. (F) Summary of the mobile fraction (Mf) ratio for different GFP linked CFTRs.

760 Data are shown as mean ± SD with individual data points. Treatments were compared by one-way
761 ANOVA with Tukey's post hoc analyses; Significantly different **: $p<0.01$; ***: $p<0.001$. (n=8-
762 13 from 1 CFBE BMI-1 donor: F508del/F508del)
763
764 **Figure 3. Characterisation of primary differentiated NHBE:CFBE mixed culture and CFBE**
765 **cell models. (A)** Schematic diagram of the NHBE:CFBE mixed culture model. CFBE and NHBE
766 from male (XY) or female (XX) donors were combined in ratios of 10%, 25%, 50% and 75%
767 NHBE:CFBE and seeded onto semipermeable membranes. (B) Confocal microscope images
768 (Maximal projection) of a representative 50% NHBE:CFBE, stained with phalloidin (red; F-actin),
769 Anti-β-tubulin (yellow; cilia), DAPI (blue; nuclei) and composite image. Scale bars are depicted
770 in the bottom right-hand corner. (C) Relative proportions of AMELX and AMELY regions in
771 genomic DNA from three different mixes of male (M) and female (F) NHBE or CF donors post-
772 functional analysis, as determined via droplet digital PCR. Data were normalised to values from
773 100% male or 100% female cultures, samples were run in duplicate (n=28). Each data point
774 represents the mean ± SD (some error bars are smaller than the symbol height). (D) Schematic
775 diagram of the lentiviral constructs used for CFTR transduction. (E) Confocal microscope images
776 of GFP CFTR transduced CFBE cultures, immunostained with phalloidin (F-actin; red), anti-β-
777 tubulin (cilia; yellow), GFP (transduced cells; green) and composite image with DAPI (blue). (F)
778 Relationship between % seeded transduced cells and % final transduced (4 hours prior to

779 functional testing) for the different CFTR cDNAs. The ratio of % final transduced to % seeded
780 transduced (%T/%S) for each CFTR is given in a table below the graph.
781
782 **Figure 4. CFTR function in primary differentiated NHBE:CFBE mixed culture and CFBE**
783 **cell models.** (A) Example I_{sc} traces from NHBE:CFBE and (B) from transduced CFBE (% final
784 transduction for individual CFTR variants are given) after incubation with CF Sputum and addition
785 of specific activators and inhibitors of ion transport (as below). ΔI_{sc} plotted against % Final NHBE
786 after addition of (C) $CFTR_{inh}172$ (10 μM) and summarised in (D) as ΔI_{sc} per % final NHBE or %
787 transduced cells in the culture (ΔI_{sc}/% Final). The dotted horizontal lines in C marks ASL height
788 in 100% NHBE cells in the presence of normal lung sputum (Healthy) or presence of CF sputum.
789 (E) TEER/% final transduced for WT-CFTR and hCAI-CFTR. Treatments were compared by
790 unpaired t test; Significantly different * $p<0.05$ (n=8-12 from 3 CF donors). (F) I_{sc} traces from
791 CFBE transduced with WT- or hCAI-CFTRs or GFP alone before and after addition of a
792 basolateral to apical Cl- gradient and specific activators and inhibitors of ion transport, amiloride
793 (10 μM), forskolin (10 μM), $CFTR_{inh}172$ (10 μM), and UTP (10 μM). All drugs were added
794 apically with exception of forskolin which was added bilaterally. Direction of chloride
795 concentration gradients (using physiological Cl^- and Cl^- free buffers) are indicated and the duration
796 of application are presented as grey bars. ΔI_{sc}/% final transduced for in response to forskolin and
797 $CFTR_{inh}172$ are given in a table below the graph.

798

799 **Figure 5. K978C-CFTR more efficiently restores ASL height and pH to differentiated CFBE**
800 **than WT CFTR**

801 (A) Representative XZ images of airway surface liquid (ASL) labelled with dextran (red layer)
802 overlying transduced CFBE following incubation with CF sputum. Transduced cells express
803 cytosolic GFP (green). (B) ASL height, after exposure to CF sputum and stimulation with
804 vasoactive intestinal peptide (VIP), plotted against % final NHBE or % final transduced CFBE for
805 CFTR variants. Dotted lines show linear regression for each CFTR variant (n=8-11 from 3 CF
806 donors). The dotted horizontal line marks ASL height in 100% NHBE cells in the presence of
807 normal lung sputum. Labelled arrows show % final transduction of K978C-CFTR required to
808 reach this value. (C) Summary of ASL height in µm per % final NHBE or % final transduced
809 CFBE in culture (µm/%Final) after exposure to CF sputum and VIP. Data are shown as mean +/-
810 SD with individual data points (n=6-13 from 3 CF donors and 6 non-CF donors). (D) ASL height
811 measured exposed to CF sputum or NHBE exposed to normal lung sputum before (-) or after (+)
812 treatment with VIP. Data are shown as mean +/- SD with individual data points (n=6-15 from 3
813 CF donors and 6 non-CF donors). Mixed-effects analysis with Sidak's post hoc analyses was used
814 to compare -VIP to +VIP, significantly different †††: $p<0.001$. (E) ASL pH per final % of NHBE
815 or CFTR transduction in culture (ΔpH/%Final). Data are shown as mean +/- SD with individual
816 data points for n=8-11 from 3 CF donors. Treatments were compared by two-way ANOVA with

817 Tukey's post hoc analyses; significantly increased as compared to CFBE are shown *: $p<0.05$. *:

818 $p<0.05$; **: $p<0.01$; ***: $p<0.001$

819

Figure 1

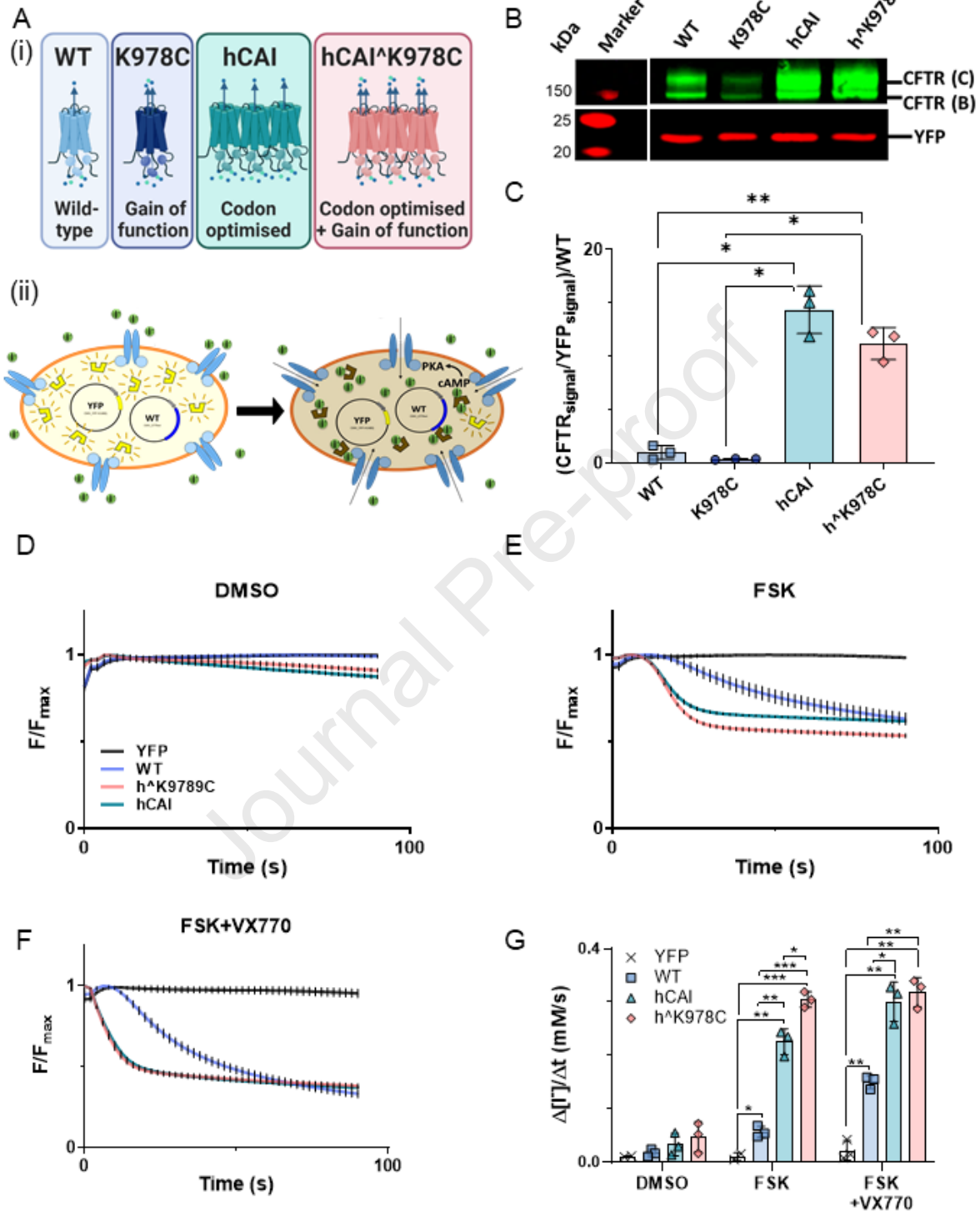

Figure 2

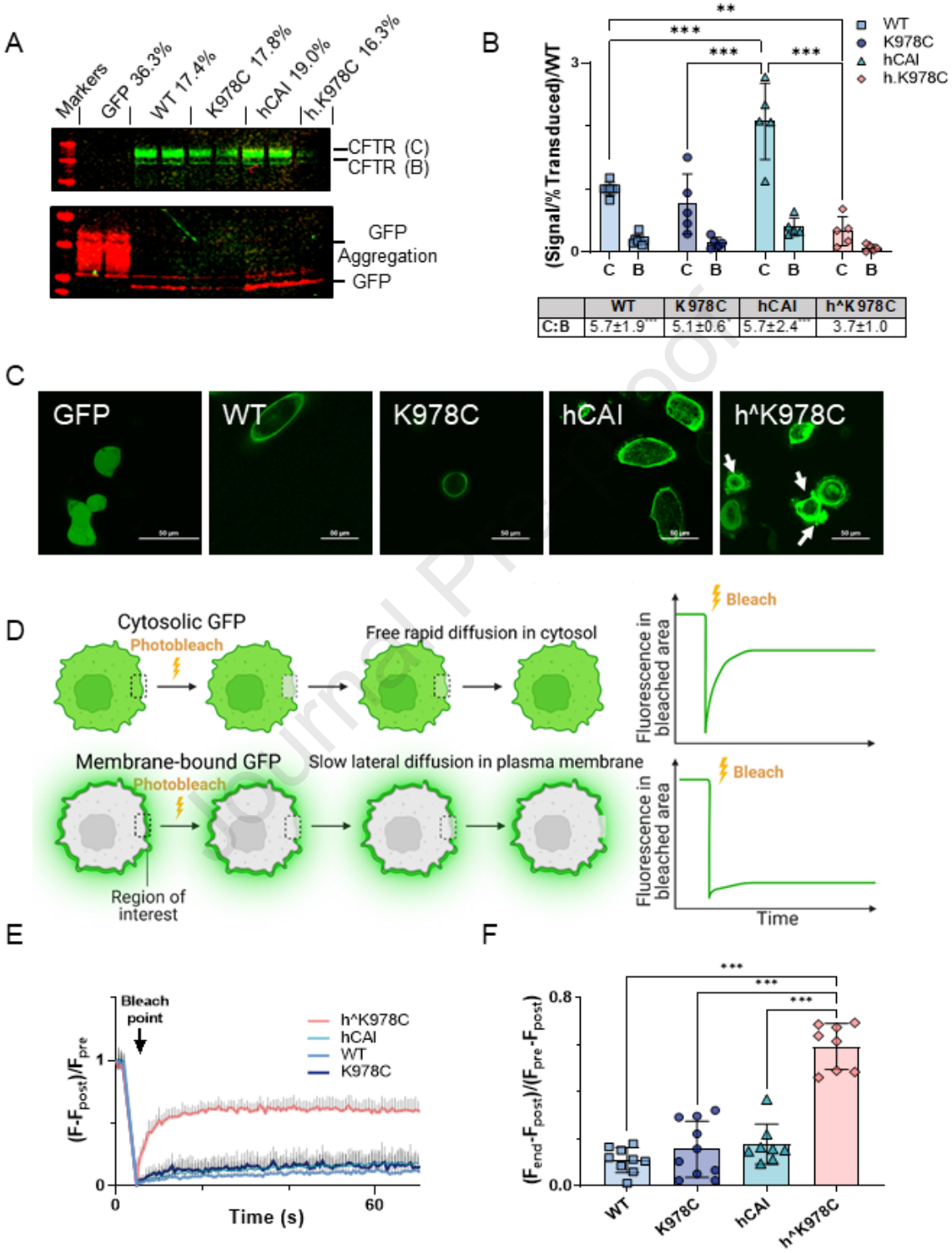
A
Markers
GFP 36.3%
WT 17.4%
K978C 17.8%
hCAI 19.0%
h.K978C 16.3%
CFTR (C)
CFTR (B)
GFP Aggregation
GFP
B
(Signal/% Transduced)/WT
WT
K978C
hCAI
h.K978C
C B C B C B C B
WT | K978C | hCAI | h^K978C
C:B | 5.7±1.9*** | 5.1±0.6* | 5.7±2.4*** | 3.7±1.0
C
GFP
WT
K978C
hCAI
h^K978C
D
Cytosolic GFP
Photobleach
Free rapid diffusion in cytosol
Bleach
Fluorescence in bleached area
Membrane-bound GFP
Photobleach
Slow lateral diffusion in plasma membrane
Region of interest
Time
E
Bleach point
h^K978C
hCAI
WT
K978C
(F-Fpost)/Fpre
Time (s)
F
(Fend-Fpost)/(Fpre-Fpost)
WT
K978C
hCAI
h^K978C

Figure 3

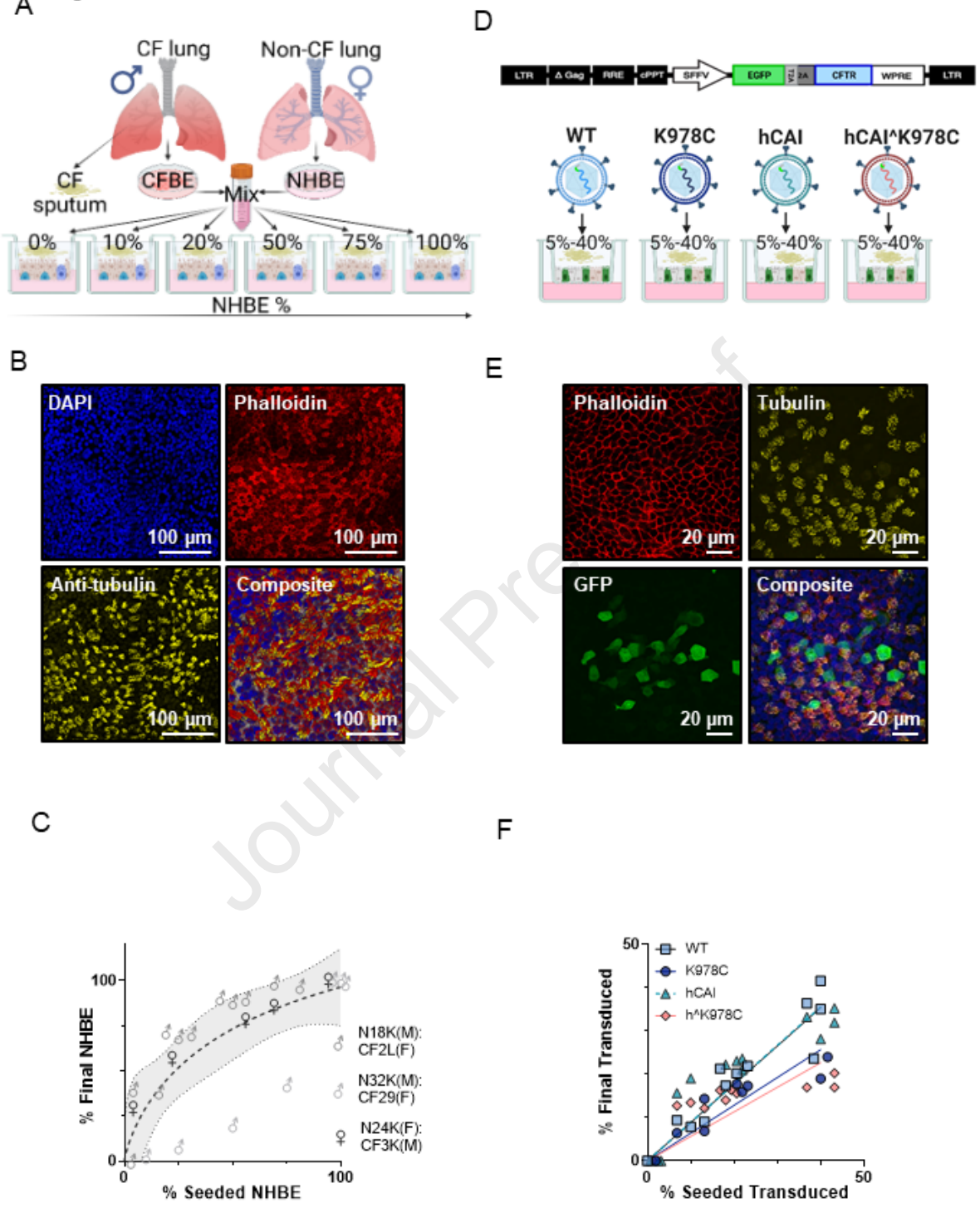
A
CF lung
Non-CF lung
CF sputum
CFBE
Mix
NHBE
0%
10%
20%
50%
75%
100%
NHBE %
D
LTR
Δ Gag
RRE
cPPT
SFFV
EGFP
T2A
CFTR
WPRE
LTR
WT
K978C
hCAI
hCAI^K978C
5%-40%
B
DAPI
Phalloidin
Anti-tubulin
Composite
100 μm
E
Phalloidin
Tubulin
GFP
Composite
20 μm
C
% Final NHBE
% Seeded NHBE
N18K(M): CF2L(F)
N32K(M): CF29(F)
N24K(F): CF3K(M)
F
% Final Transduced
% Seeded Transduced
WT
K978C
hCAI
h^K978C

Figure 4

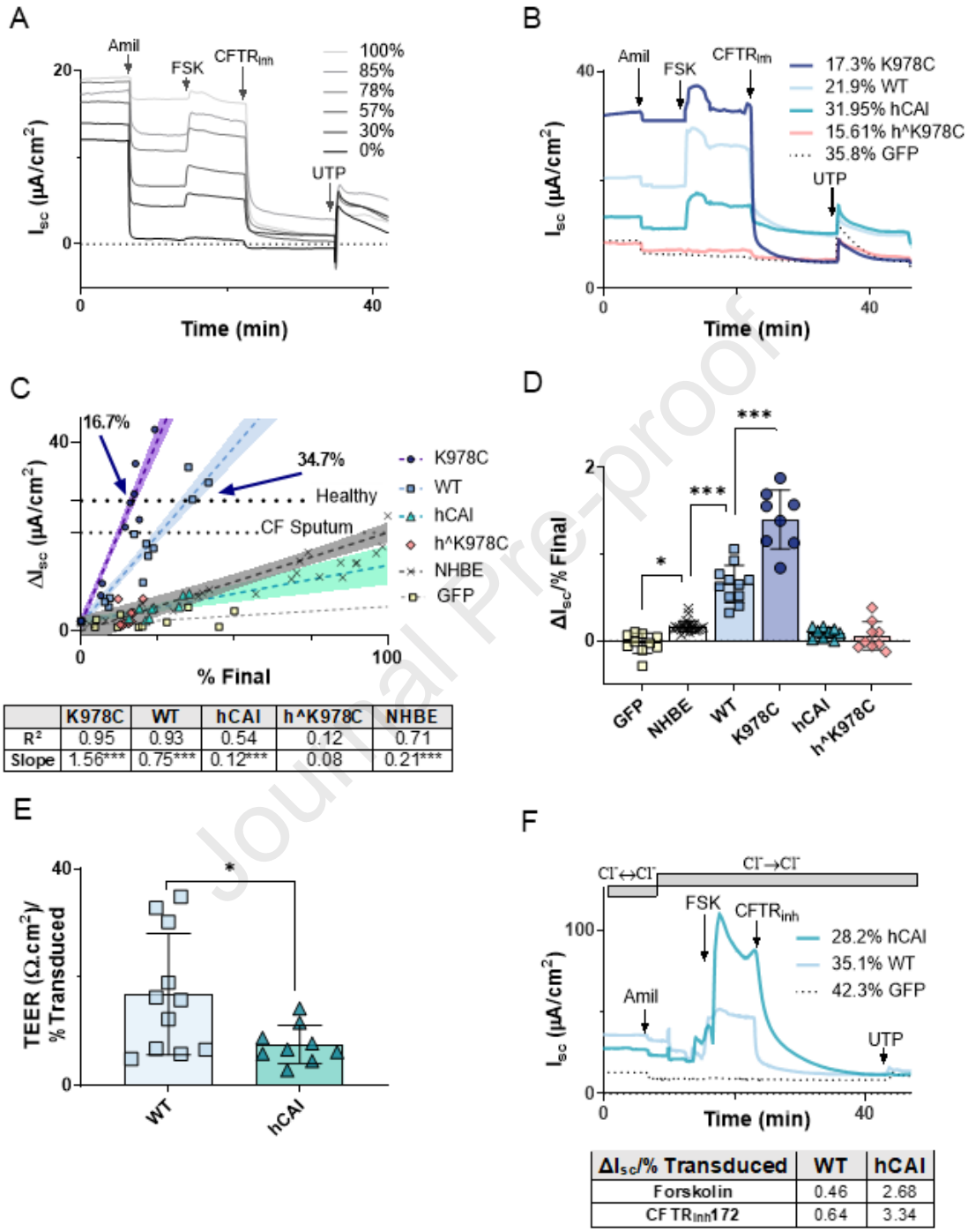

	K978C	WT	hCAI	h^K978C	NHBE
R^2	0.95	0.93	0.54	0.12	0.71
Slope	1.56***	0.75***	0.12***	0.08	0.21***

ΔI_{sc}/% Transduced	WT	hCAI
Forskolin	0.46	2.68
$CFTR_{Inh}172$	0.64	3.34

Figure 5

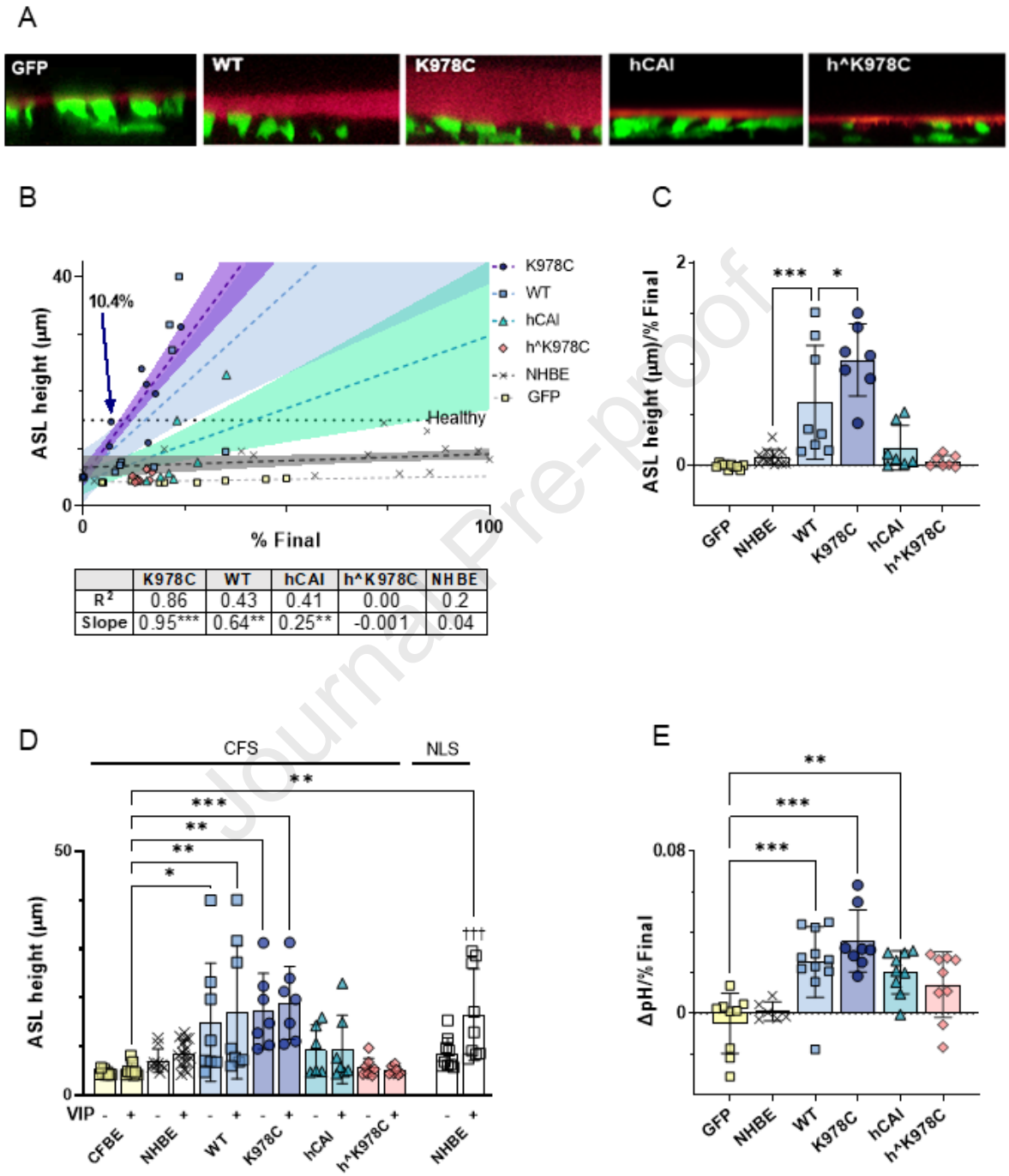

	K978C	WT	hCAI	h^K978C	NHBE
R^2	0.86	0.43	0.41	0.00	0.2
Slope	0.95***	0.64**	0.25**	-0.001	0.04

Baines and colleagues show that viral delivery of cystic fibrosis transmembrane regulator (CFTR) gain of function variant cDNA (K978C-CFTR) to cystic fibrosis bronchial epithelial cells (CFBE), in the presence of CF sputum, was more effective at restoring anion secretion, ASL hydration and pH than wild type CFTR.